Diagnosis of Planar Phased Arrays Through a Probabilistic Compressive Sensing Approach

M. Salucci, A. Gelmini, G. Oliveri, and A. Massa

Abstract

This work deals with the detection of faulty elements in planar phased antenna arrays starting from far-field pattern measurements. Owing to the intrinsically *sparse* nature of the problem unknowns at hand, the diagnosis problem is formulated as a probabilistic Compressive Sensing (*CS*) one and it is effectively and efficiently solved through a customized Bayesian *CS* (*BCS*) solution approach. Some representative synthetic benchmarks are shown in order to verify the potentialities as well as the current limitations of the proposed *BCS*-based diagnosis tool, as well as to assess its flexibility in dealing with arbitrary excitation taperings of the *AUT.*

Contents

1 Numerical Validation

1.1 Bayliss Array, $N = 316$, Isotropic Sources

Parameters

- Gold Array
  - Total number of elements: $N = 316$;
  - Type of elements: isotropic/ideal [1];
  - Spacing along x and y: $d_x = d_y = 0.5$ [λ];
  - Excitation tapering: Bayliss;
    - Radius: $R = 5$ [λ];
    - Transition index: $t = 3$;
    - Peak sidelobe level: $PSL = 25$ [dB];

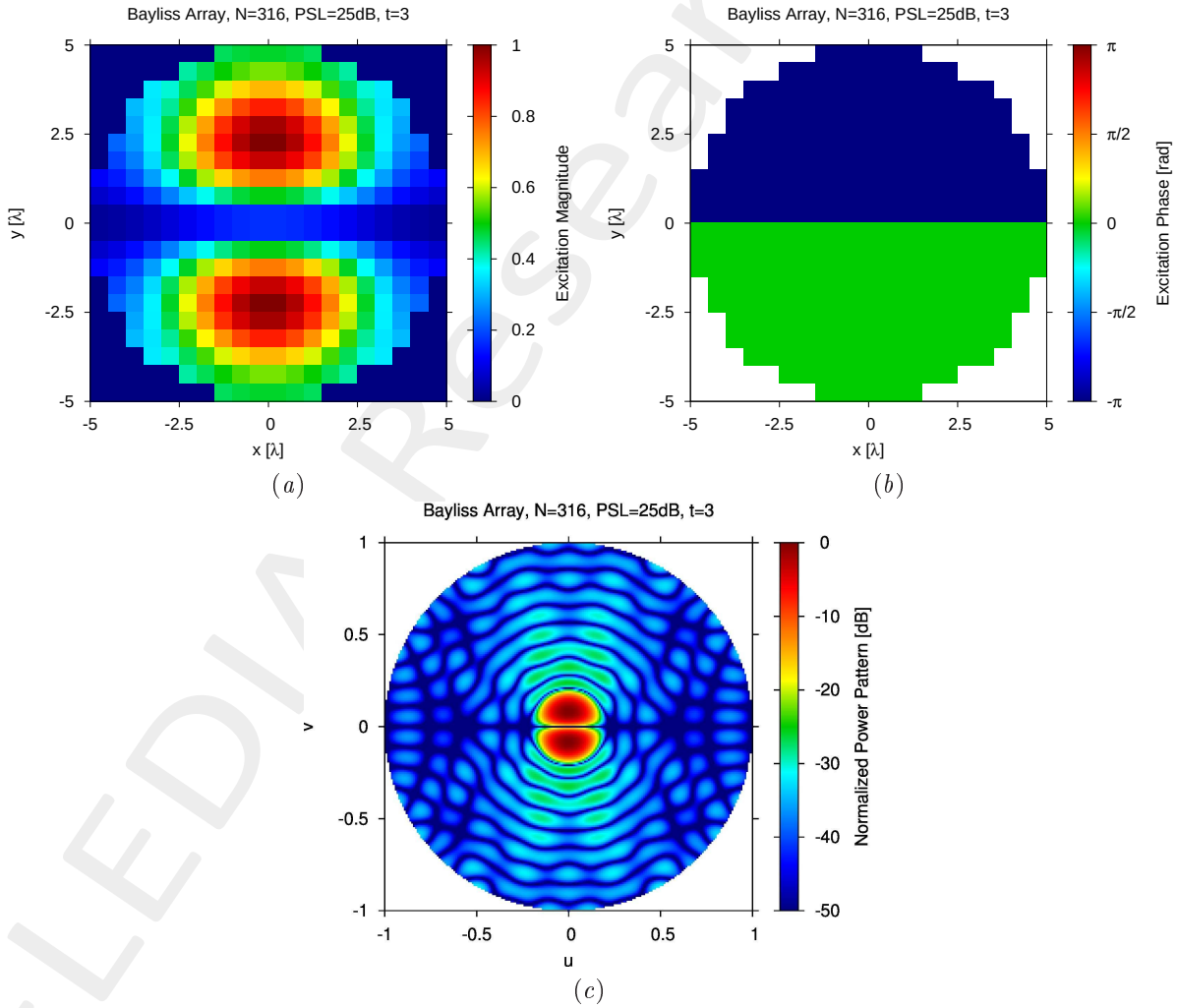

Figure 1: (a) magnitude and (b) phase of the array excitations; (c) normalized power pattern.

[1] In order to model *isotropic* radiators, let us assume that the embedded elements patterns are equal to $F_\theta^{(n)}(u, v) = 1$ and $F_\varphi^{(n)}(u, v) = 0$, for $n = 1, ..., N$.

- Failed Array
  - Failure factor: $\kappa = 0$ (total failures);
  - Failure rate: see table below;

N_f	$\Phi = \frac{N_f}{N}$
3	1%
6	2%
13	4%
25	8%
51	16%

Table 1: Number of failures (N_f) and corresponding failure rate ($\Phi = \frac{N_f}{N}$).

- Measurement set-up
  - Type of sampling: uniform sampling in the (u, v) plane;
  - Number of points in the visible range: $K = 317$;
  - Ratio between measurements and number of elements: $\nu = \frac{K}{N} \simeq 1.0$ ($\nu^{(opt)}$);
- *BCS* solver
  - Noise variance: $\eta = 5 \times 10^{-1}$ ($\eta^{(opt)}$);
  - Tolerance factor: $\iota = 10^{-8}$;
- Signal-to-Noise-Ratio: $SNR = \{10; 20; ...; 100\}$.

Results

$\Phi = \frac{N_f}{N} = 1\%$ $(N_f = 3)$ - **Best and Worst** BCS **Reconstructions**

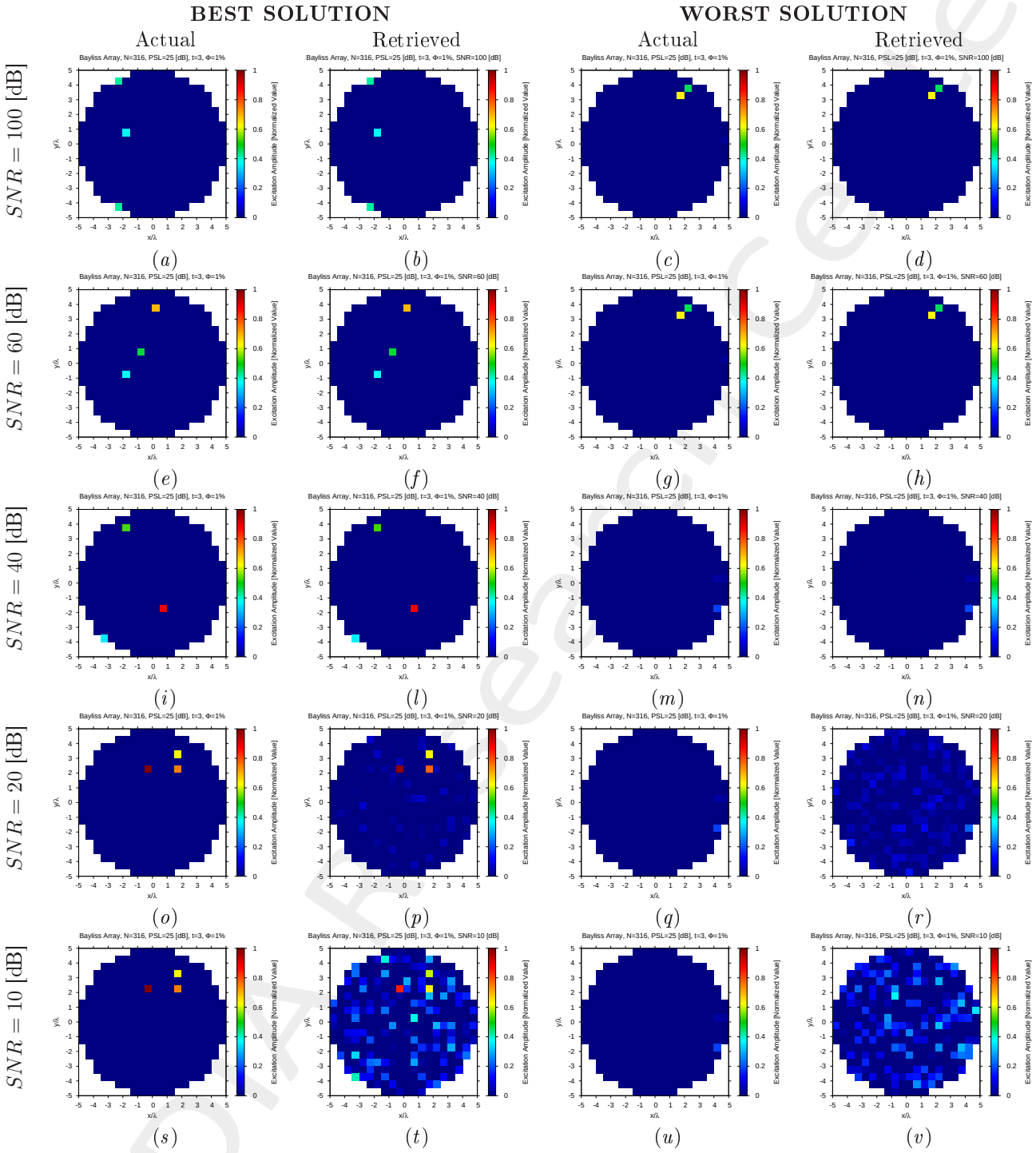

Figure 2: Bayliss Array ($N = 316$, $PSL = 25$ [dB], $t = 3$, $\Phi = 1\%$) - Best and worst reconstructions by BCS under several SNR values.

$\Phi = \frac{N_f}{N} = 2\%$ $(N_f = 6)$ - **Best and Worst** BCS **Reconstructions**

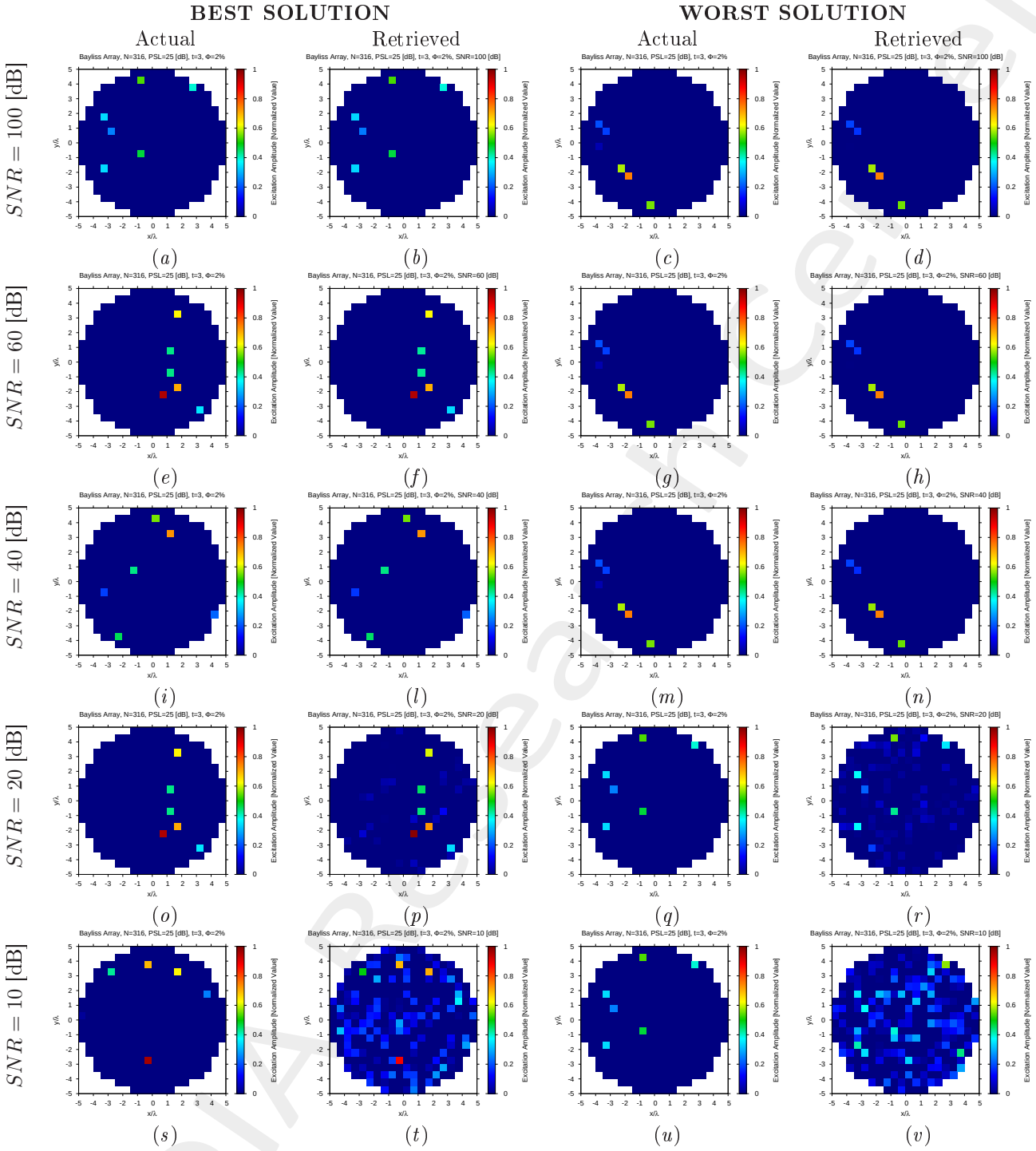

Figure 3: Bayliss Array ($N = 316$, $PSL = 25$ [dB], $t = 3$, $\Phi = 2\%$) - Best and worst reconstructions by BCS under several SNR values.

$\Phi = \frac{N_f}{N} = 4\%$ $(N_f = 13)$ - **Best and Worst** BCS **Reconstructions**

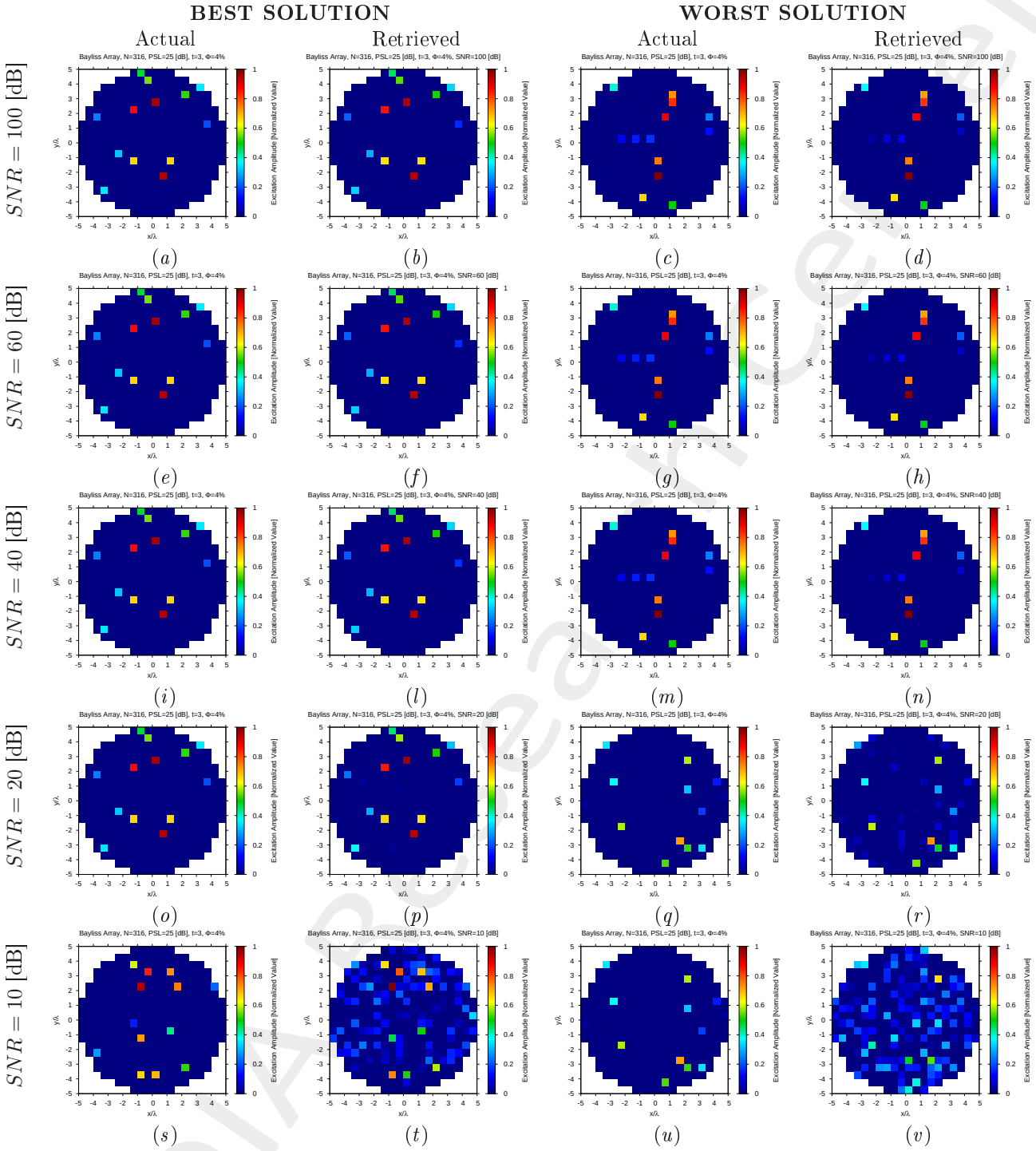

Figure 4: Bayliss Array ($N = 316$, $PSL = 25$ [dB], $t = 3$, $\Phi = 4\%$) - Best and worst reconstructions by BCS under several SNR values.

$\Phi = \frac{N_f}{N} = 8\%$ $(N_f = 25)$ - **Best and Worst** BCS **Reconstructions**

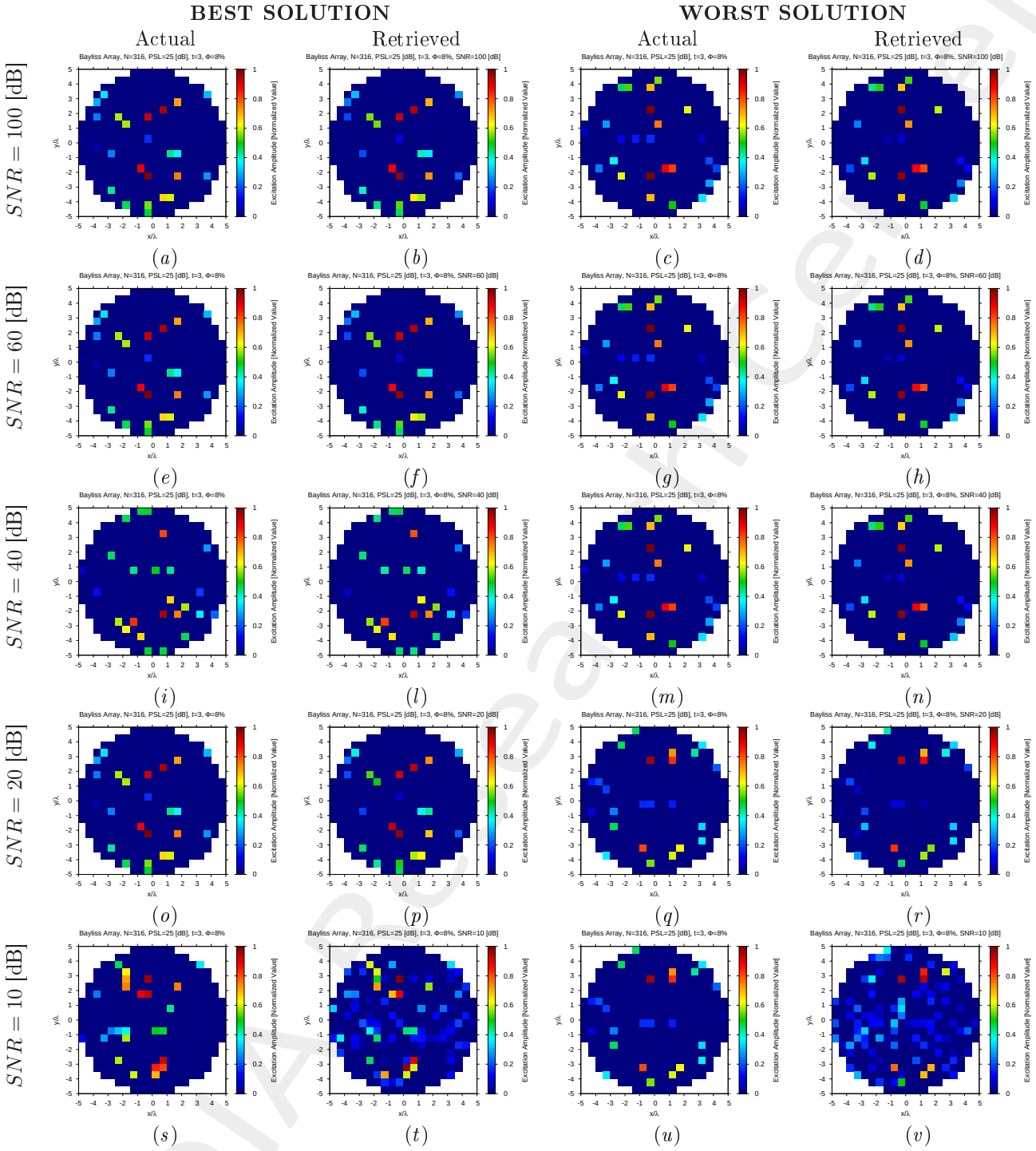

Figure 5: Bayliss Array ($N = 316$, $PSL = 25$ [dB], $t = 3$, $\Phi = 8\%$) - Best and worst reconstructions by BCS under several SNR values.

$\Phi = \frac{N_f}{N} = 16\%$ $(N_f = 51)$ - **Best and Worst** BCS **Reconstructions**

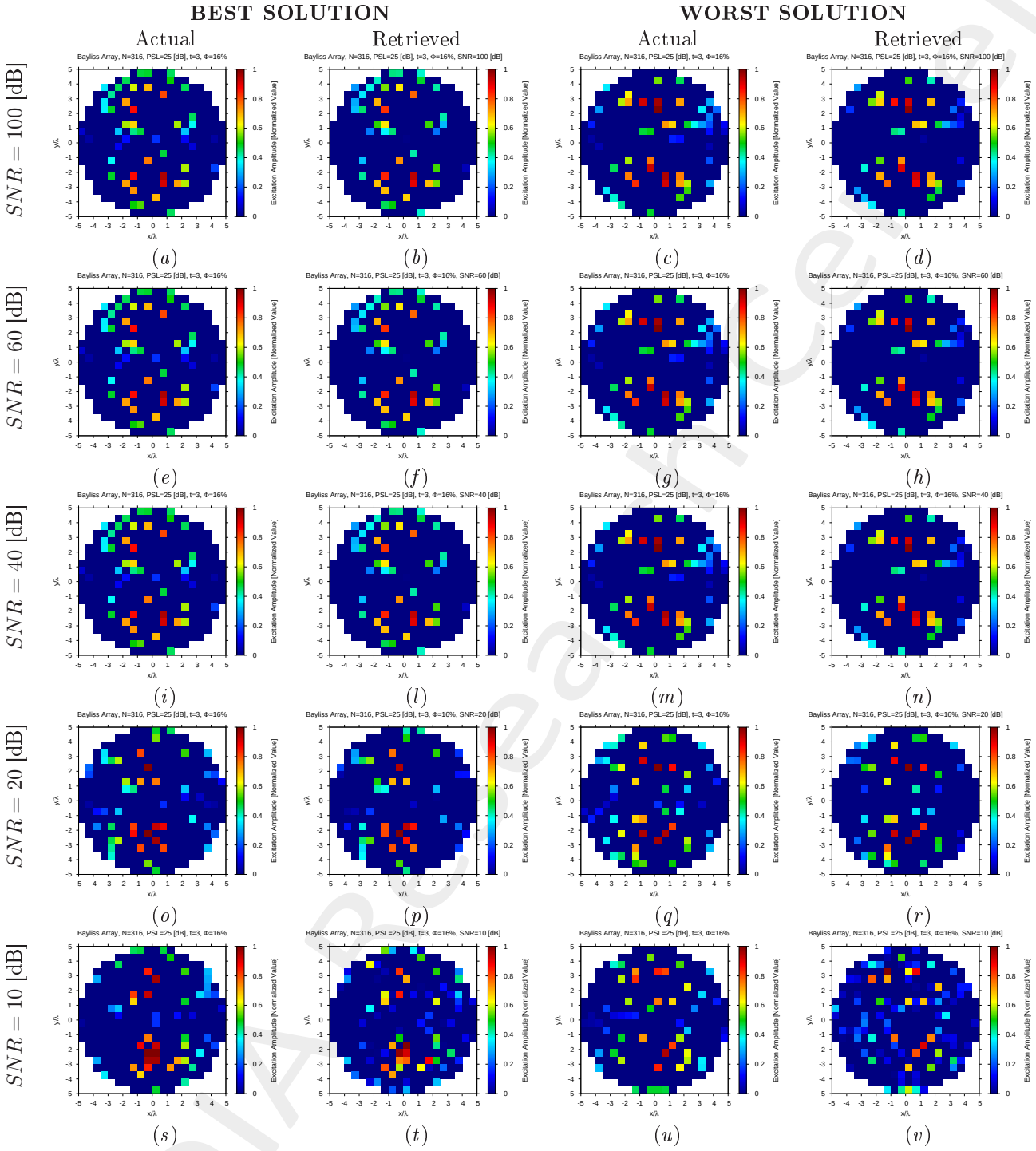

Figure 6: Bayliss Array ($N = 316$, $PSL = 25$ [dB], $t = 3$, $\Phi = 16\%$) - Best and worst reconstructions by BCS under several SNR values.

Diagnosis Error and Confidence Level

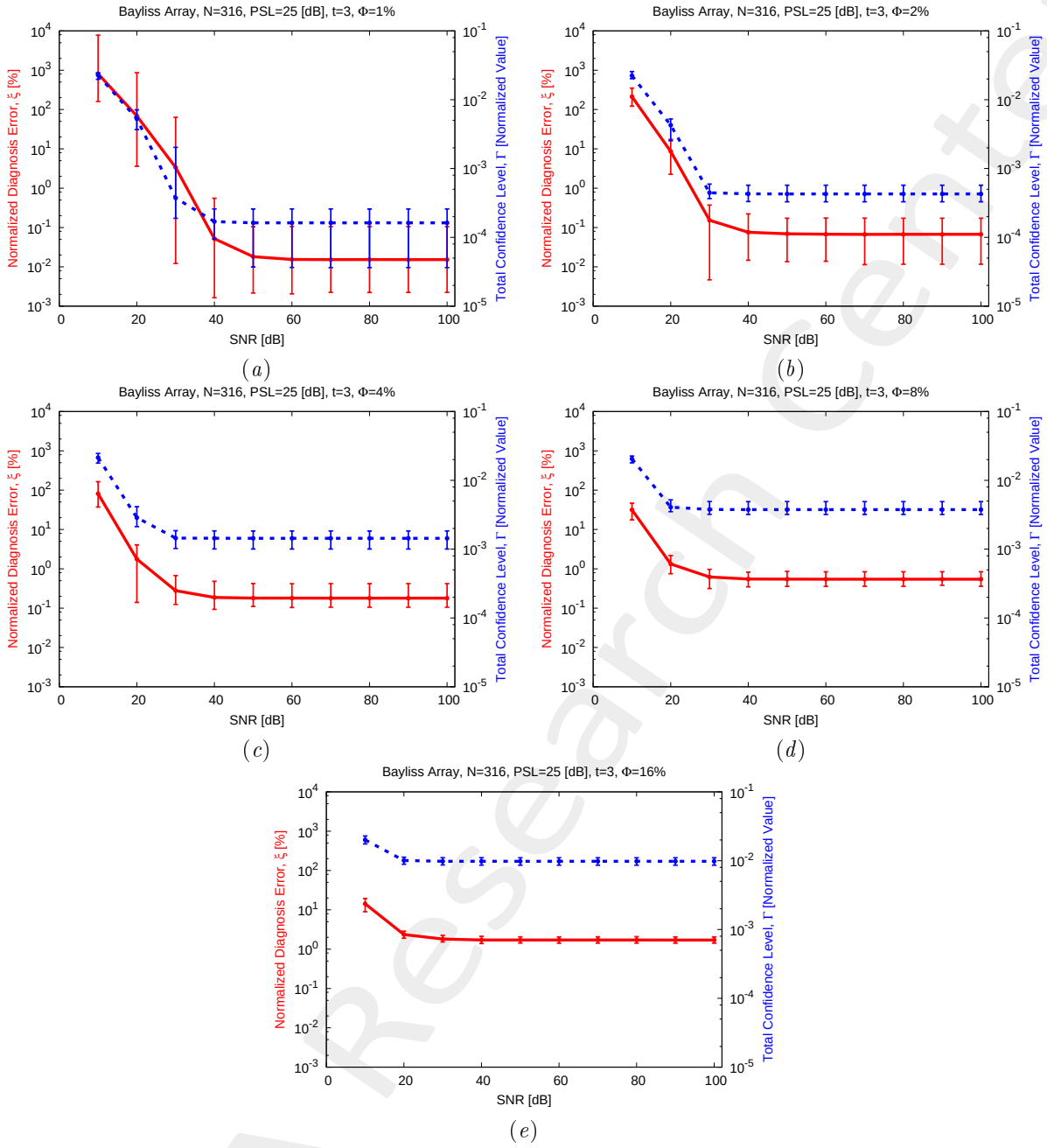

Figure 7: Bayliss Array ($N = 316$, $PSL = 25$ [dB], $t = 3$) - Behavior of the average, minimum and maximum diagnosis error (ξ) and total confidence level (Γ) versus the SNR, for (a) $\Phi = 1\%$, (b) $\Phi = 2\%$, (c) $\Phi = 4\%$, (d) $\Phi = 8\%$, and (e) $\Phi = 16\%$.

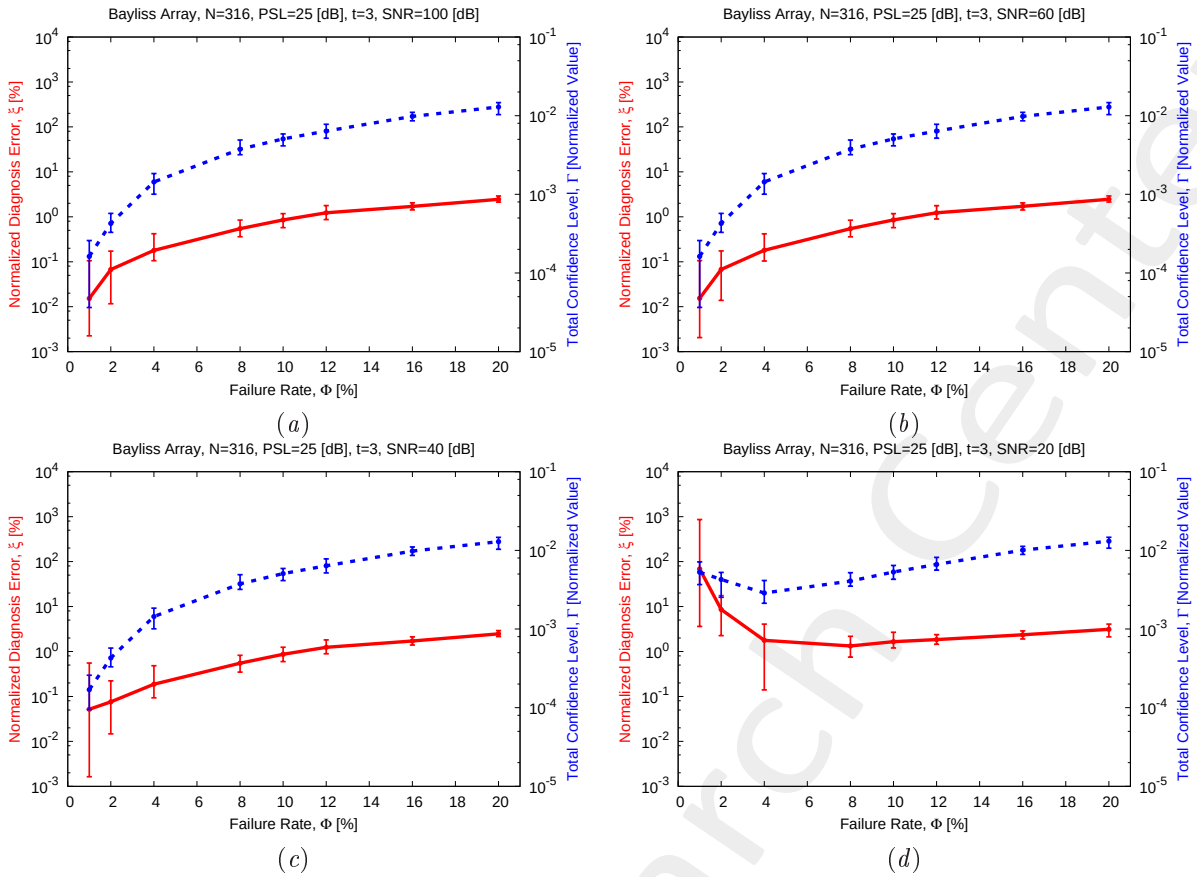

Figure 8: Bayliss Array ($N = 316$, $PSL = 25$ [dB], $t = 3$) - Behavior of the average, minimum and maximum diagnosis error (ξ) and total confidence level (Γ) versus the failure rate (Φ), for (a) $SNR = 100$ [dB], (b) $SNR = 60$ [dB], (c) $SNR = 40$ [dB], and (d) $SNR = 20$ [dB].

1.2 Slepian Array, $N = 400$, Isotropic Sources

Parameters

- Gold Array
  - Total number of elements: $N = 400$;
  - Type of elements: isotropic/ideal [2]
  - Spacing along x and y: $d_x = d_y = 0.5$ $[\lambda]$;
  - Excitation tapering: Slepian;
    - Angular region at the receiver: $\Psi = \{(u, v) : -u_0 \leq u \leq u_0, -v_0 \leq v \leq v_0\}$, with $u_0 = v_0 = 0.1$.

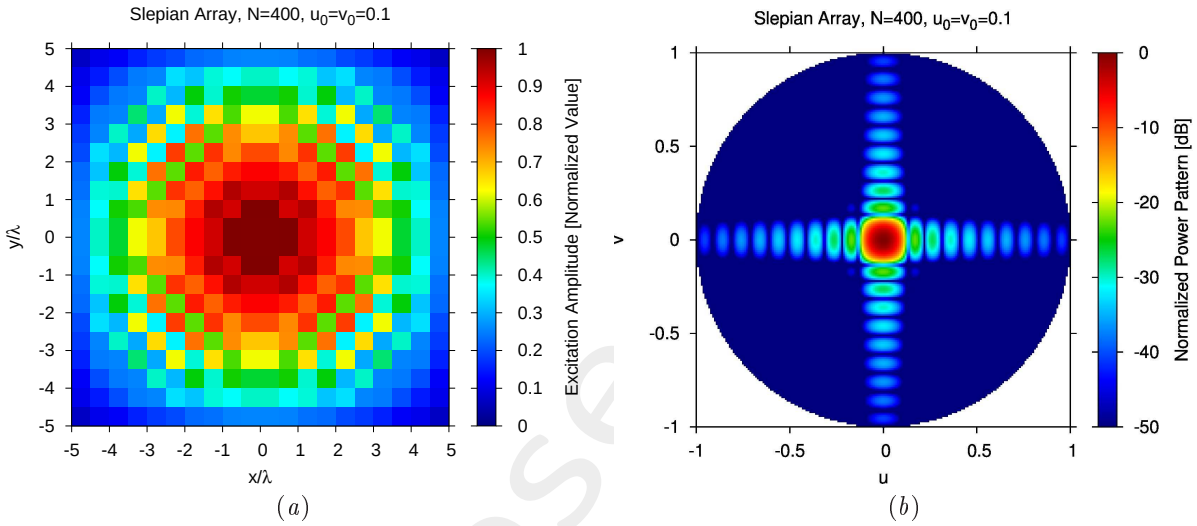

(a) (b)

Figure 9: (a) Array excitations and (b) normalized power pattern of the gold array.

- Failed Array
  - Failure factor: $\kappa = 0$ (total failures);
  - Failure rate: see table below;

N_f	$\Phi = \frac{N_f}{N}$
4	1%
8	2%
16	4%
32	8%
64	16%

Table 2: Number of failures (N_f) and corresponding failure rate ($\Phi = \frac{N_f}{N}$).

- Measurement set-up

[2] In order to model *isotropic* radiators, let us assume that the embedded elements patterns are equal to $F_\theta^{(n)}(u, v) = 1$ and $F_\varphi^{(n)}(u, v) = 0$, for $n = 1, ..., N$.

  - Type of sampling: uniform sampling in the (u, v) plane;
  - Number of points in the visible range: $K = 408$;
  - Ratio between measurements and number of elements: $\nu = \frac{K}{N} \simeq 1.0$ $(\nu^{(opt)})$;

- *BCS* solver
  - Noise variance: $\eta = 5 \times 10^{-1}$ $(\eta^{(opt)})$;
  - Tolerance factor: $\iota = 10^{-8}$;

- Signal-to-Noise-Ratio: $SNR = \{10; 20; ...; 100\}$.

$\Phi = \frac{N_f}{N} = 1\%$ $(N_f = 4)$ - **Best and Worst** BCS **Reconstructions**

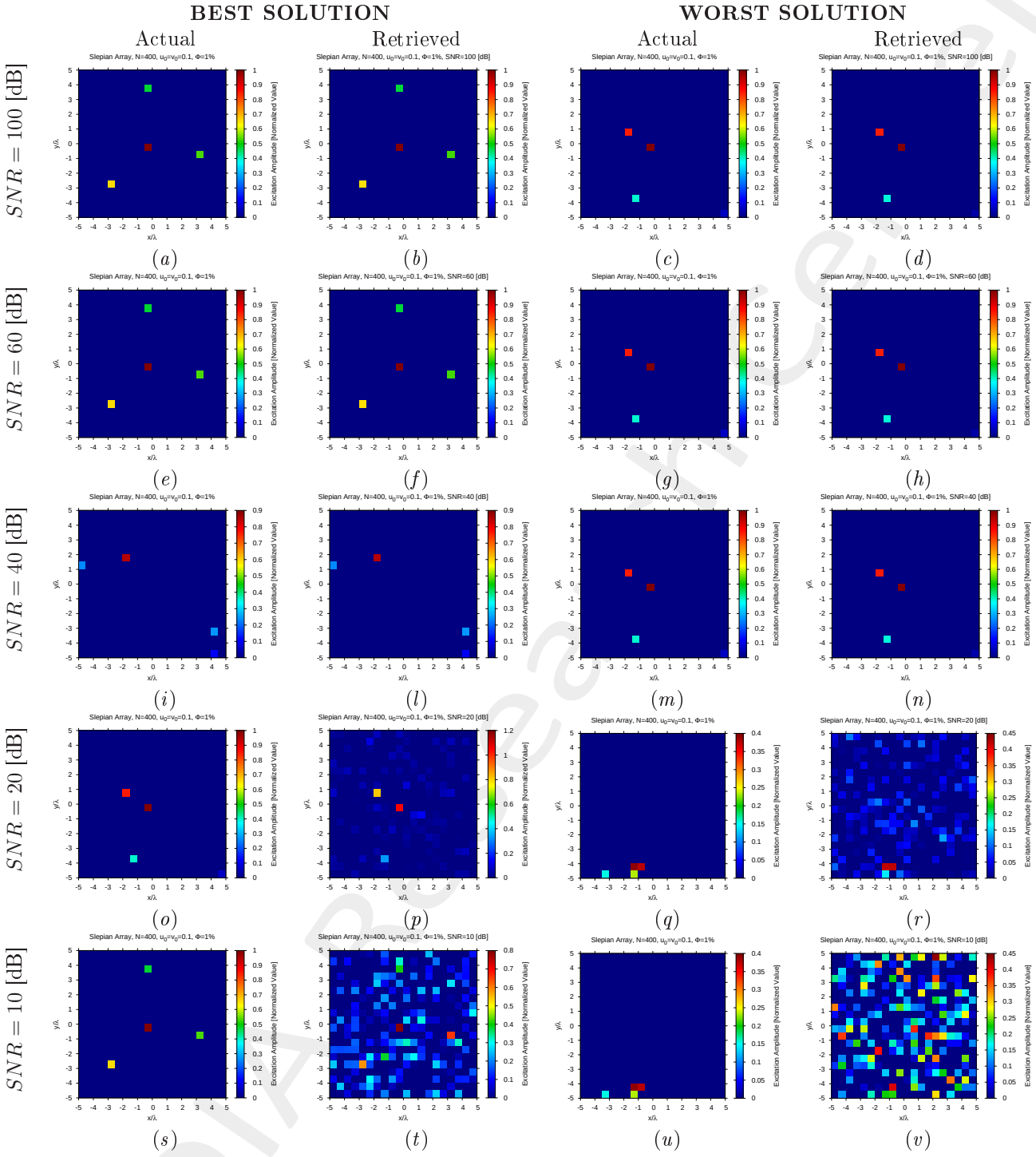

Figure 10: Slepian Array ($N = 400$, $u_0 = v_0 = 0.1$, $\Phi = 1\%$) - Best and worst reconstructions by BCS under several SNR values.

$\Phi = \frac{N_f}{N} = 2\%$ $(N_f = 8)$ - **Best and Worst** BCS **Reconstructions**

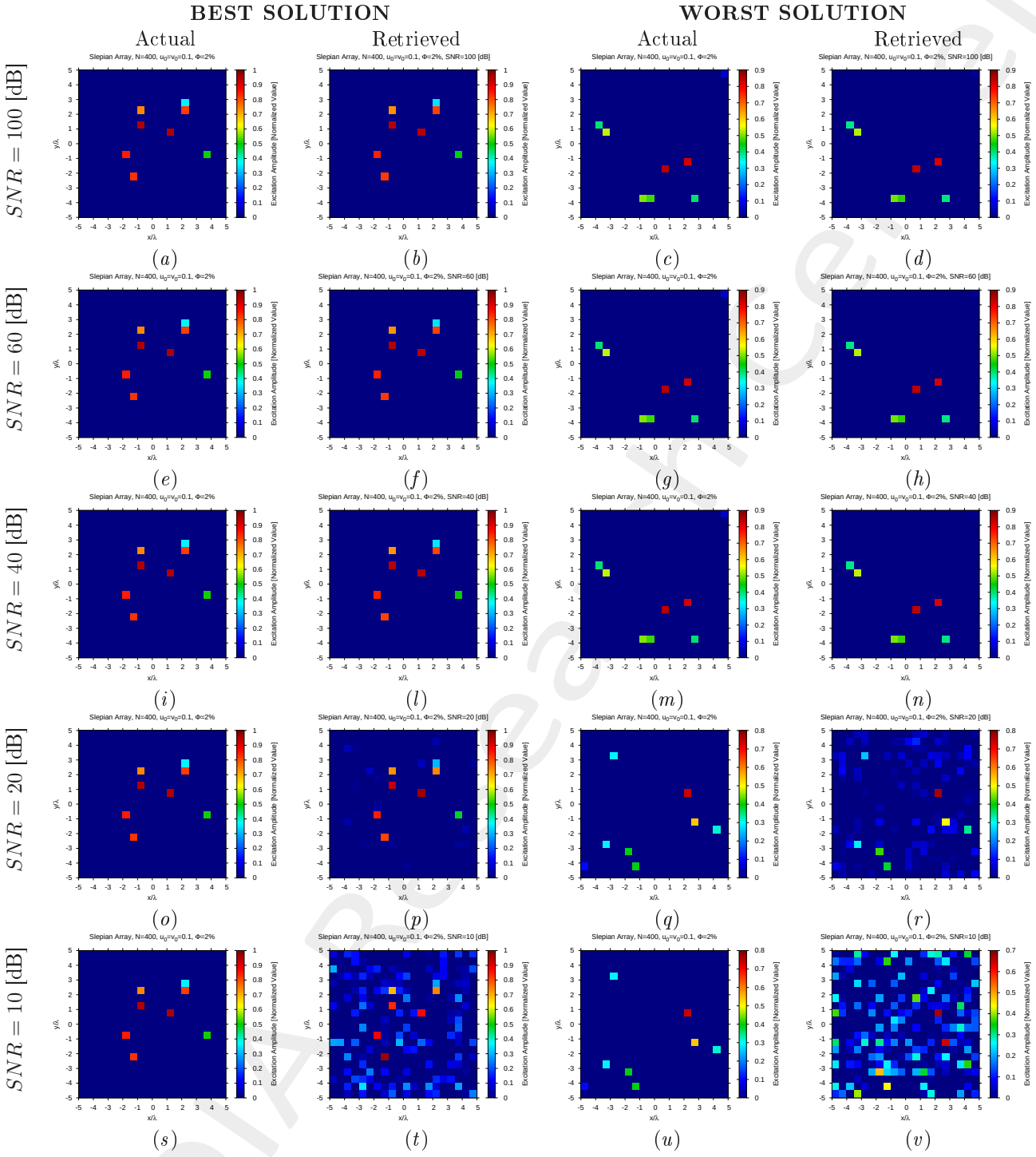

Figure 11: Slepian Array ($N = 400$, $u_0 = v_0 = 0.1$, $\Phi = 2\%$) - Best and worst reconstructions by BCS under several SNR values.

$\Phi = \frac{N_f}{N} = 4\%$ $(N_f = 16)$ - **Best and Worst** BCS **Reconstructions**

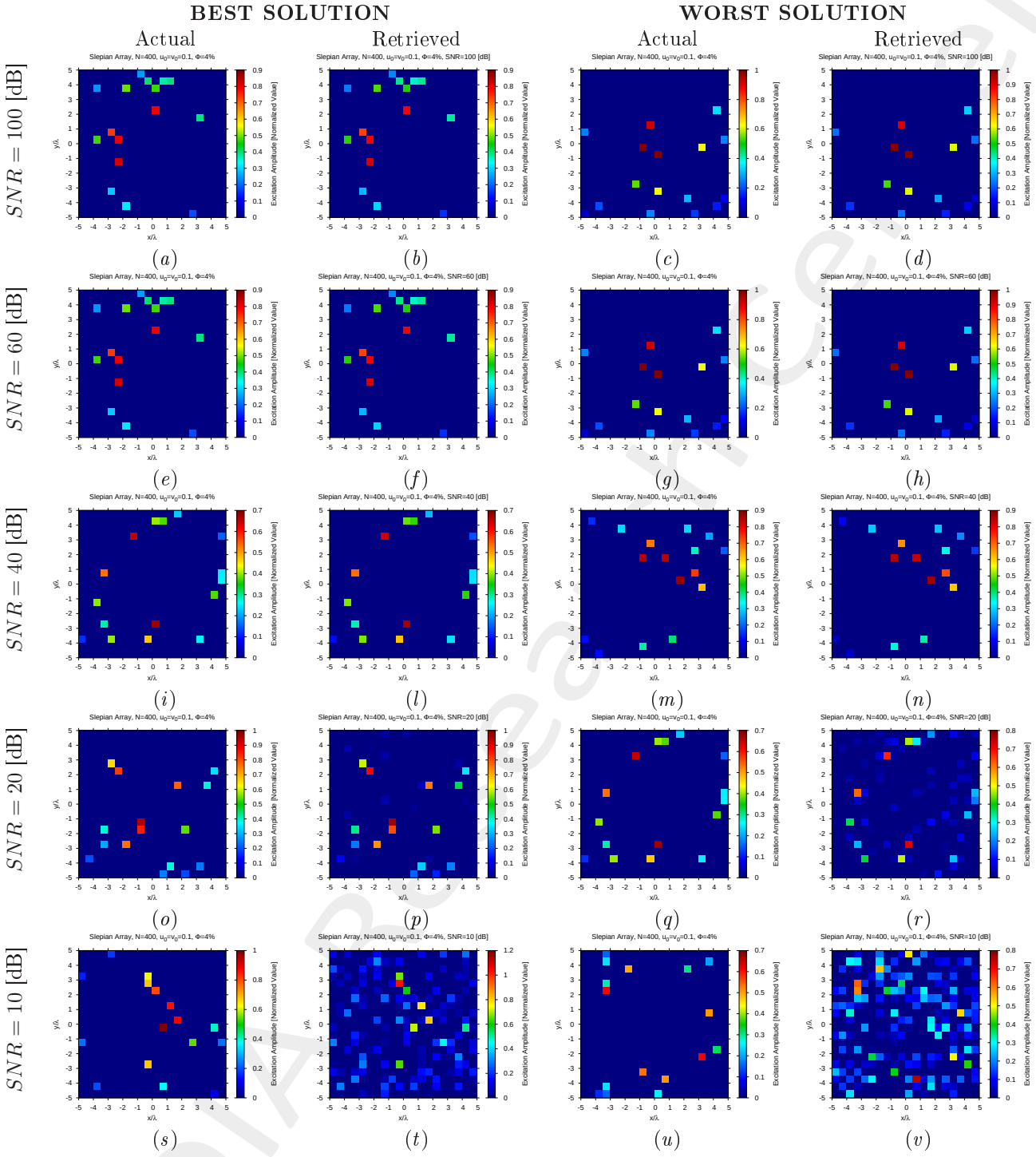

Figure 12: Slepian Array ($N = 400$, $u_0 = v_0 = 0.1$, $\Phi = 4\%$) - Best and worst reconstructions by BCS under several SNR values.

$\Phi = \frac{N_f}{N} = 8\%$ $(N_f = 32)$ - **Best and Worst** BCS **Reconstructions**

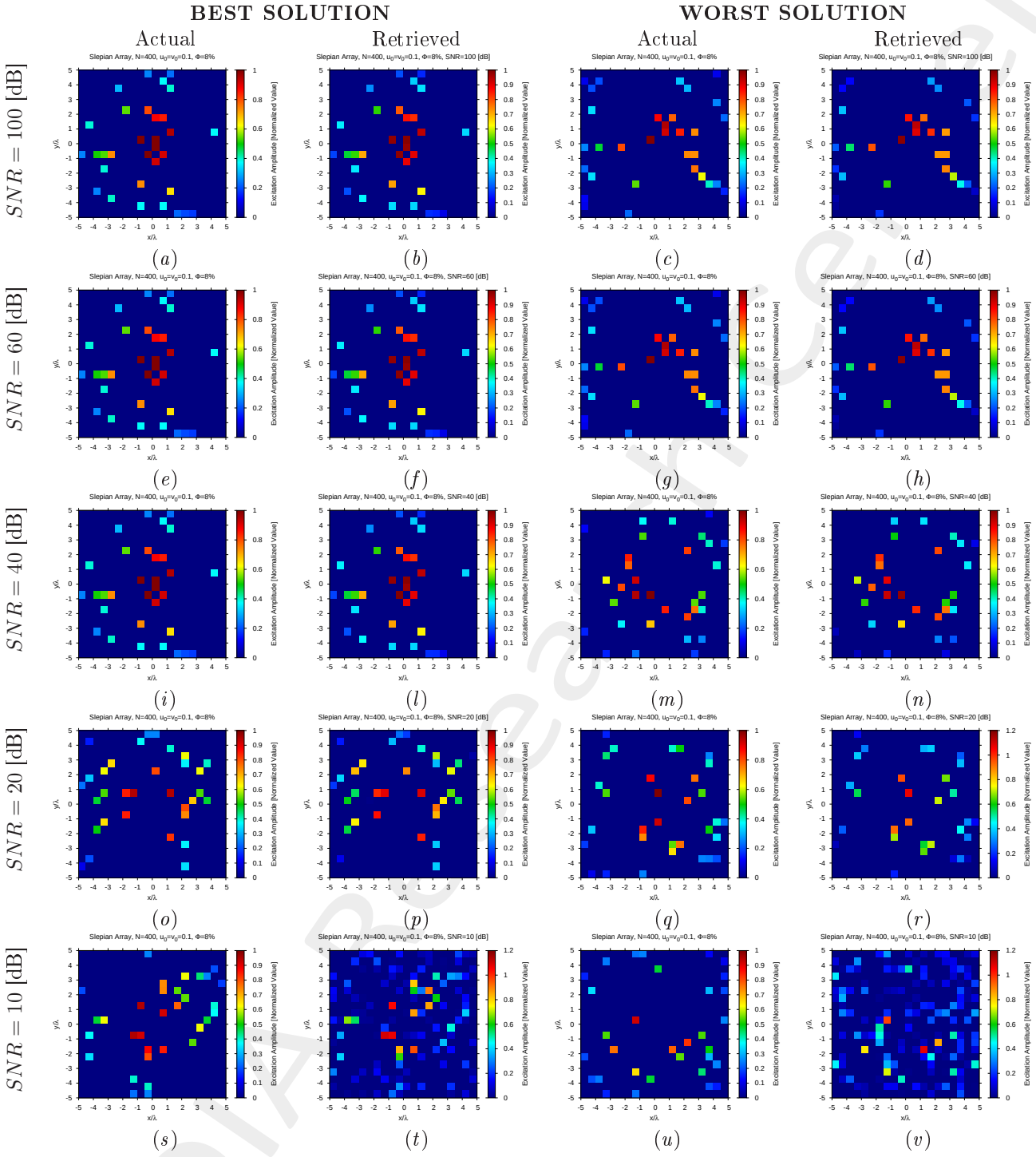

Figure 13: Slepian Array ($N = 400$, $u_0 = v_0 = 0.1$, $\Phi = 8\%$) - Best and worst reconstructions by BCS under several SNR values.

$\Phi = \frac{N_f}{N} = 16\%$ $(N_f = 64)$ - **Best and Worst** BCS **Reconstructions**

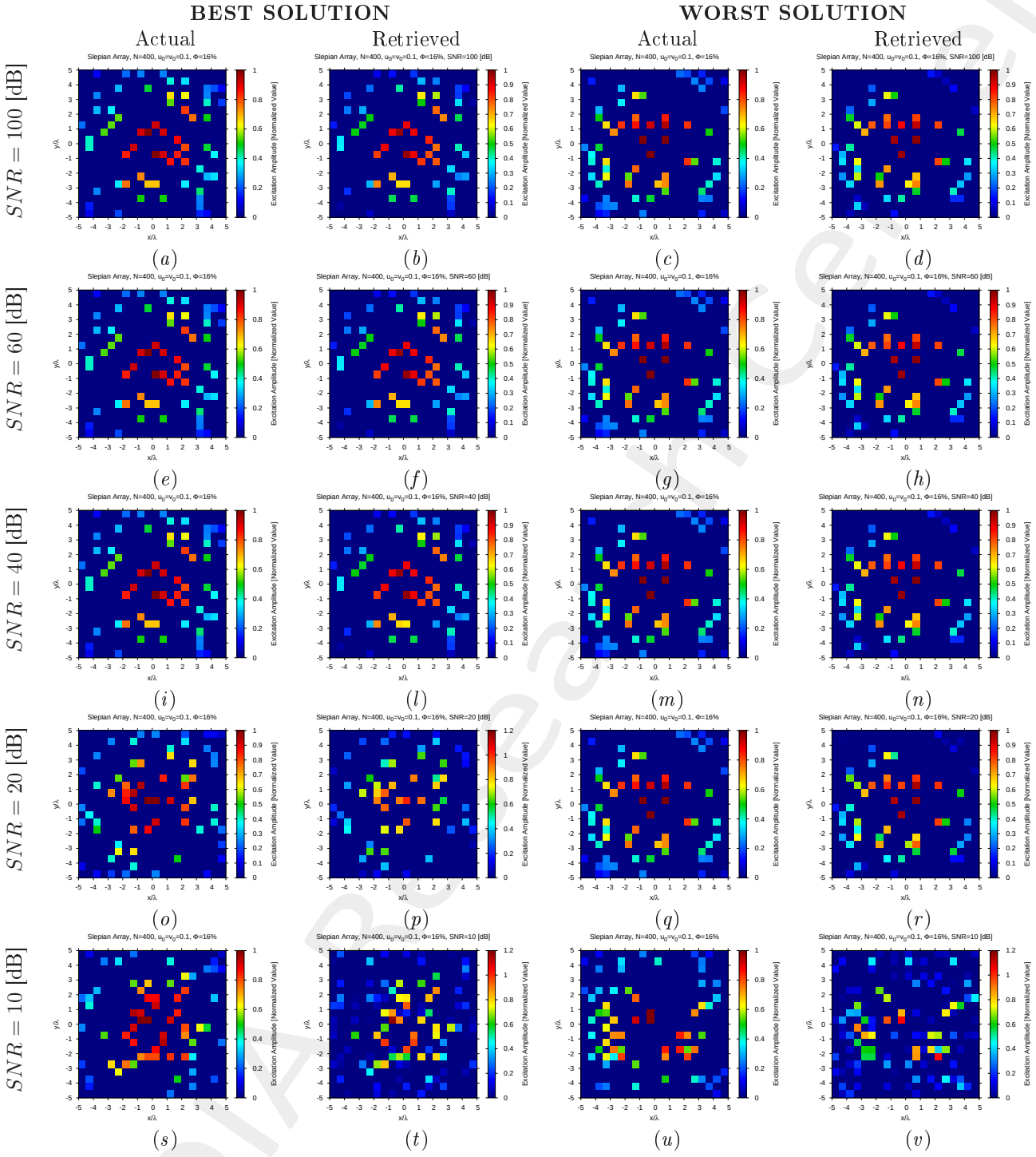

Figure 14: Slepian Array ($N = 400$, $u_0 = v_0 = 0.1$, $\Phi = 16\%$) - Best and worst reconstructions by BCS under several SNR values.

Diagnosis Error and Confidence Level

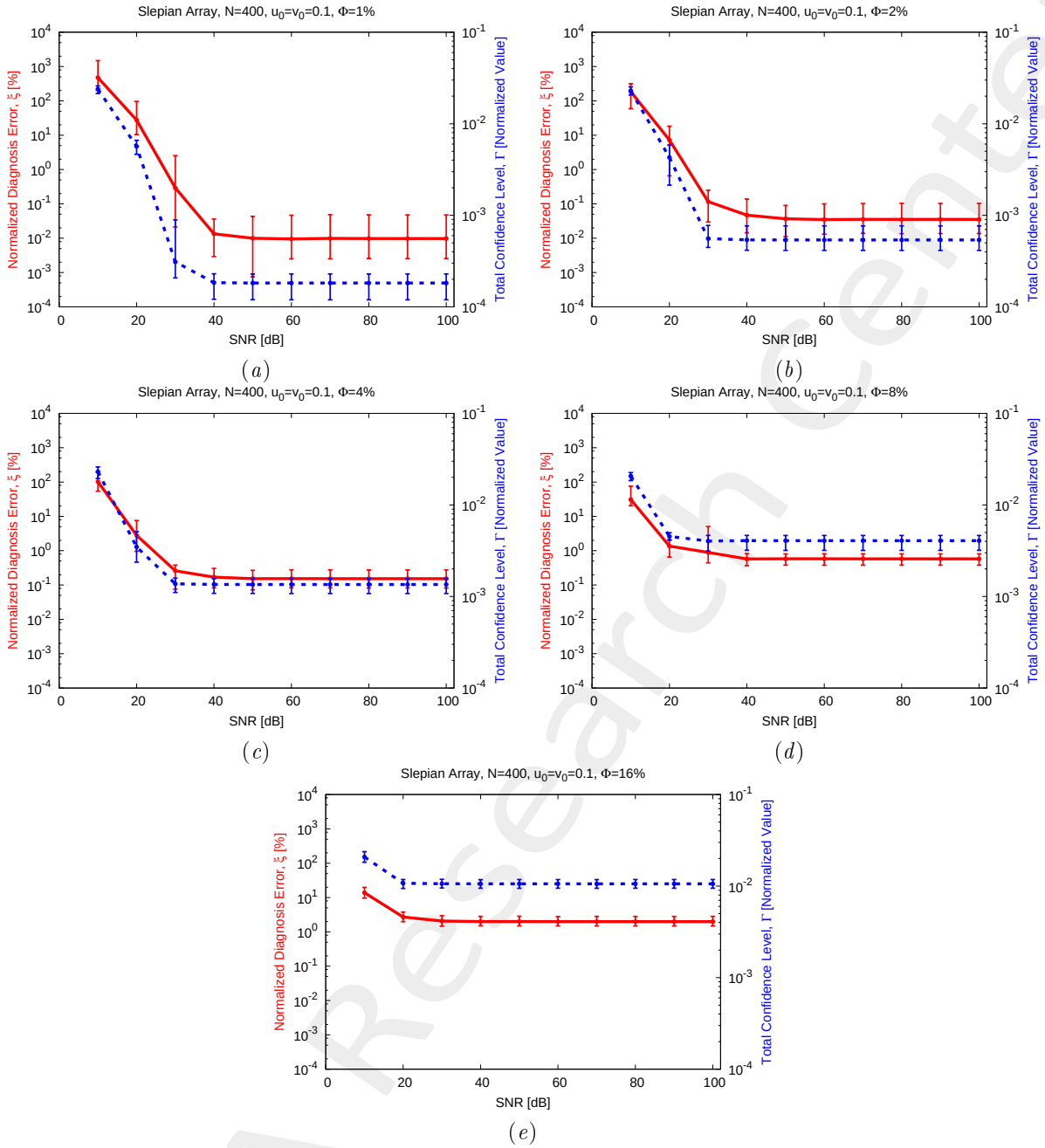

Figure 15: Slepian Array ($N = 400$, $u_0 = v_0 = 0.1$) - Behavior of the average, minimum and maximum diagnosis error (ξ) and total confidence level (Γ) versus the SNR, for (a) $\Phi = 1\%$, (b) $\Phi = 2\%$, (c) $\Phi = 4\%$, (d) $\Phi = 8\%$, (e) $\Phi = 16\%$.

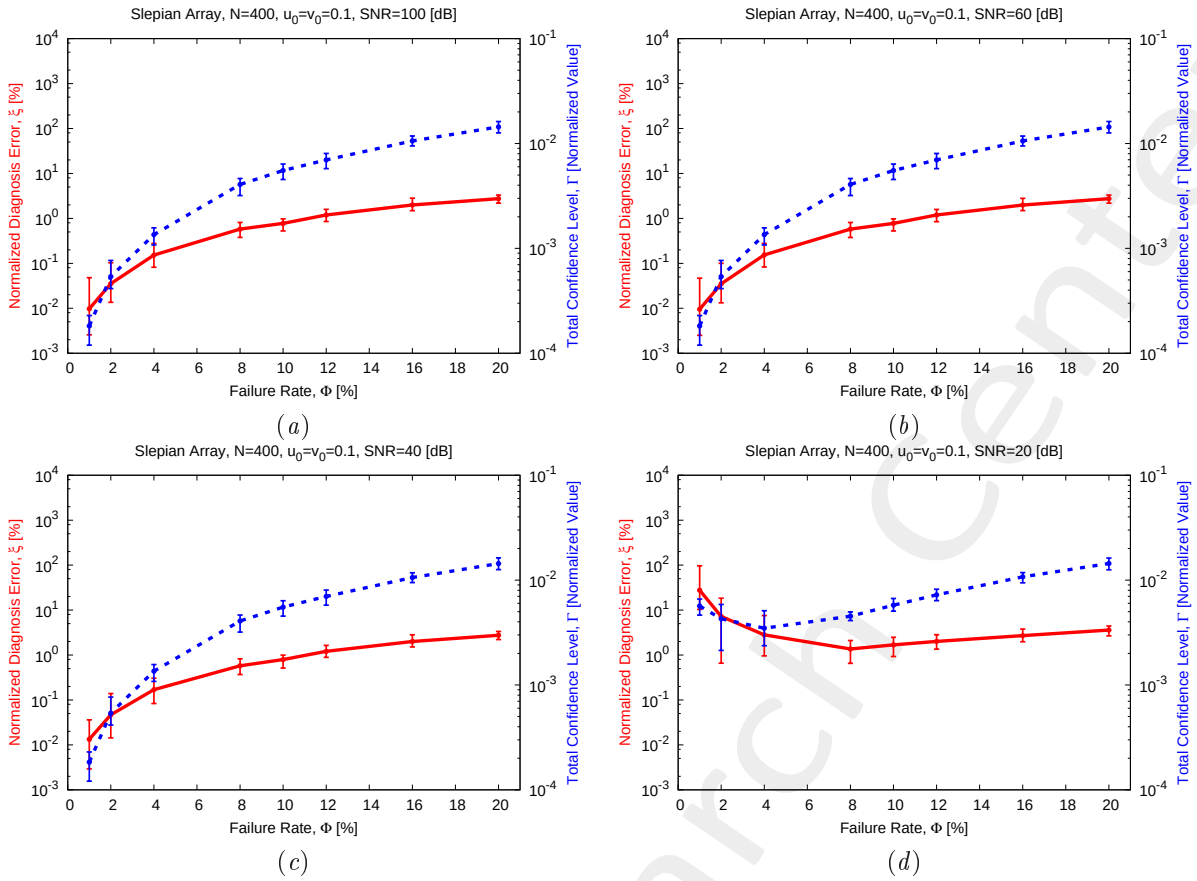

Figure 16: Slepian Array ($N = 400$, $u_0 = v_0 = 0.1$) - Behavior of the average, minimum and maximum diagnosis error (ξ) and total confidence level (Γ) versus the failure rate (Φ), for (a) $SNR = 100$ [dB], (b) $SNR = 60$ [dB], (c) $SNR = 40$ [dB], and (d) $SNR = 20$ [dB].

References

[1] P. Rocca, G. Oliveri, R. J. Mailloux, and A. Massa, "Unconventional phased array architectures and design methodologies - A Review," *Proc. IEEE*, vol. 104, no. 3, pp. 544-560, Mar. 2016.

[2] G. Oliveri, G. Gottardi, F. Robol, A. Polo, L. Poli, M. Salucci, M. Chuan, C. Massagrande, P. Vinetti, M. Mattivi, R. Lombardi, and A. Massa, "Co-design of unconventional array architectures and antenna elements for *5G* base stations," *IEEE Trans. Antennas Propag.*, vol. 65, no. 12, pp. 6752-6767, Dec. 2017.

[3] G. Oliveri, P. Rocca, and A. Massa, "Reliable diagnosis of large linear arrays - a Bayesian compressive sensing approach," *IEEE Trans. Antennas Propag.*, vol. 60, no. 10, pp. 4627-4636, Oct. 2012.

[4] M. Salucci, A. Gelmini, G. Oliveri, and A. Massa, "Planar arrays diagnosis by means of an advanced Bayesian compressive processing," *IEEE Trans. Antennas Propag.*, vol. 66, no. 11, pp. 5892-5906, Nov. 2018.

[5] A. Massa, P. Rocca, and G. Oliveri, "Compressive sensing in electromagnetics - A review," *IEEE Antennas Propag. Mag.*, pp. 224-238, vol. 57, no. 1, Feb. 2015.

[6] G. Oliveri, M. Salucci, N. Anselmi, and A. Massa, "Compressive sensing as applied to inverse problems for imaging: theory, applications, current trends, and open challenges," *IEEE Antennas Propag. Mag.,* vol. 59, no. 5, pp. 34-46, Oct. 2017.

[7] P. Rocca, M. A. Hannan, M. Salucci, and A. Massa, "Single-snapshot DoA estimation in array antennas with mutual coupling through a multi-scaling Bayesian compressive sensing strategy," *IEEE Trans. Antennas Propag.*, vol. 65, no. 6, pp. 3203-3213, Jun. 2017.

[8] M. Carlin, P. Rocca, G. Oliveri, F. Viani, and A. Massa, "Directions-of-arrival estimation through Bayesian Compressive Sensing strategies," *IEEE Trans. Antennas Propag.*, vol. 61, no. 7, pp. 3828-3838, Jul. 2013.

[9] L. Poli, G. Oliveri, P. Rocca, M. Salucci, and A. Massa, "Long-distance WPT unconventional arrays synthesis," *J. Electromagn. Waves Appl.*, vol. 31, no. 14, pp. 1399-1420, Jul. 2017.

[10] G. Oliveri, M. Salucci, and A. Massa, "Synthesis of modular contiguously clustered linear arrays through a sparseness-regularized solver," *IEEE Trans. Antennas Propag.*, vol. 64, no. 10, pp. 4277-4287, Oct. 2016.

[11] G. Oliveri and A. Massa, "Bayesian compressive sampling for pattern synthesis with maximally sparse non-uniform linear arrays," *IEEE Trans. Antennas Propag.*, vol. 59, no. 2, pp. 467-481, Feb. 2011.

[12] N. Anselmi, G. Oliveri, M. A. Hannan, M. Salucci, and A. Massa, "Color compressive sensing imaging of arbitrary-shaped scatterers," *IEEE Trans. Microw. Theory Techn.*, vol. 65, no. 6, pp. 1986-1999, Jun. 2017.

[13] N. Anselmi, G. Oliveri, M. Salucci, and A. Massa, "Wavelet-based compressive imaging of sparse targets," *IEEE Trans. Antennas Propag.*, vol. 63, no. 11, pp. 4889-4900, Nov. 2015.

[14] L. Poli, G. Oliveri, F. Viani, and A. Massa, "MT-BCS-based microwave imaging approach through minimum-norm current expansion," *IEEE Trans. Antennas Propag.*, vol. 61, no. 9, pp. 4722-4732, Sep. 2013.

[15] G. Oliveri, N. Anselmi, and A. Massa, "Compressive sensing imaging of non-sparse 2D scatterers by a total-variation approach within the Born approximation," *IEEE Trans. Antennas Propag.*, vol. 62, no. 10, pp. 5157-5170, Oct. 2014.

[16] L. Poli, G. Oliveri, and A. Massa, "Imaging sparse metallic cylinders through a local shape function bayesian compressive sensing approach," *J. Opt. Soc. Am. A*, vol. 30, no. 6, pp. 1261-1272, 2013.

[17] L. Poli, G. Oliveri, P. Rocca, and A. Massa, "Bayesian compressive sensing approaches for the reconstruction of two-dimensional sparse scatterers under TE illumination," *IEEE Trans. Geosci. Remote Sens.*, vol. 51, no. 5, pp. 2920-2936, May 2013.

[18] L. Poli, G. Oliveri, and A. Massa, "Microwave imaging within the first-order Born approximation by means of the contrast-field Bayesian compressive sensing," *IEEE Trans. Antennas Propag.*, vol. 60, no. 6, pp. 2865-2879, Jun. 2012.

[19] G. Oliveri, L. Poli, P. Rocca, and A. Massa, "Bayesian compressive optical imaging within the Rytov approximation," *Opt. Lett.*, vol. 37, no. 10, pp. 1760-1762, 2012.

[20] G. Oliveri, P. Rocca, and A. Massa, "A Bayesian compressive sampling-based inversion for imaging sparse scatterers," *IEEE Trans. Geosci. Remote Sens.*, vol. 49, no. 10, pp. 3993-4006, Oct. 2011.

[21] N. Anselmi, L. Poli, G. Oliveri, and A. Massa, "Iterative multi-resolution bayesian CS for microwave imaging," *IEEE Trans. Antennas Propag.*, vol. 66, no. 7, pp. 3665-3677, Jul. 2018.

[22] L. Poli, P. Rocca, G. Oliveri, and A. Massa, "Failure correction in time-modulated linear arrays," *IET Radar, Sonar & Navigation*, vol. 8, no. 3, pp. 195-201, 2014.